Heliyon 9 (2023) e17258

Contents lists available at ScienceDirect

Heliyon

journal homepage: www.cell.com/heliyon

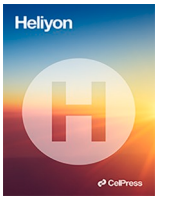

Optimization of microfibrillated cellulose isolation from cocoa pod husk via mild oxalic acid hydrolysis: A response surface methodology approach

L. Fernando Zambrano-Mite [a], Yanet Villasana [a], M. Lorena Bejarano [b], Christian Luciani [c], Dario Niebieskikwiat [c], Willin Álvarez [d], Dario F. Cueva [e], Daniel Aguilera-Pesantes [f], Lourdes M. Orejuela-Escobar [b,e,g,h,i,*]

[a] *Biomass Laboratory, Biomass to Resources Group, Universidad Regional Amazónica Ikiam, Tena 096975, Ecuador*
[b] *Institute of Energy and Materials, Universidad San Francisco de Quito USFQ, Diego de Robles y Vía Interoceánica, Quito 170901, Ecuador*
[c] *Departamento de Física, Colegio de Ciencias e Ingenierías, Universidad San Francisco de Quito USFQ, Diego de Robles y Vía Interoceánica, Quito 170901, Ecuador*
[d] *Facultad de Ciencias de La Vida. Universidad Regional Amazónica Ikiam, Tena 096975, Ecuador*
[e] *Applied Circular Engineering & Simulation Group (GICAS), Chemical Engineering Department, Colegio de Ciencias e Ingenierías, Universidad San Francisco de Quito USFQ, Diego de Robles y Vía Interoceánica, Quito 170901, Ecuador*
[f] *CLYDENT S.A, km 4.5 Vía a Taura, Guayaquil, Ecuador*
[g] *Instituto de Investigaciones Biológicas y Ambientales (Biósfera), Universidad San Francisco de Quito USFQ, Diego de Robles y Vía Interoceánica, Quito 170901, Ecuador*
[h] *Instituto de Investigaciones Biomédicas (IBioMed), Universidad San Francisco de Quito USFQ, Diego de Robles y Vía Interoceánica, Quito 170901, Ecuador*
[i] *Geocircular Consulting Group LLC, Temple Terrace, FL 33617, USA*

ARTICLE INFO

Keywords:
Cocoa pod husk
Design of experiments
Green hydrolysis
Microfibrillated cellulose
Biomass valorization

ABSTRACT

Theobroma cacao L. species, cultivated worldwide for its valuable beans, generates up to 72% weight of the fruit as waste. The lack of reutilization technologies in the cocoa agroindustry has hindered the exploitation of valuable bio-components applicable to the generation of high value added bioproducts. One such bioproduct is microfibrillated cellulose (MFC), a biopolymer that stands out for its desirable mechanical properties and biocompatibility in biomedical, packing, 3D printing, and construction applications. In this study, we isolated microfibrillated cellulose (MFC) from cocoa pod husk (CPH) via oxalic acid hydrolysis combined with a steam explosion. MFC isolation started with the Solid/Liquid extraction via Soxhlet, followed by mild citric acid hydrolysis, diluted alkaline hydrolysis, and bleaching pre-treatments. A Response Surface Methodology (RSM) was used to optimize the hydrolysis reaction at levels between 110 and 125 °C, 30–90 min at 5–10% (w/v) oxalic acid concentration. The cellulose-rich fraction was characterized by Fourier-Transform Infrared Spectroscopy (FTIR), Thermogravimetric Analysis (TGA), Differential Scanning Calorimetry (DSC), X-Ray Diffraction (XRD), and Scanning Electron Microscopy (SEM) analyses. Characterization analyses revealed a cellulose-rich polymer with fibers ranging from 6 to 10 μm, a maximum thermal degradation temperature of 350 °C, and a crystallinity index of 63.4% (peak height method) and 29.0% (amorphous subtraction method). The optimized hydrolysis conditions were 125 °C, 30 min, at 5% w/v oxalic acid: with a 75.7% yield. These results compare with MFC obtained through highly concentrated inorganic acid hydrolysis

* Corresponding author.
E-mail address: lorejuela@usfq.edu.ec (L.M. Orejuela-Escobar).

https://doi.org/10.1016/j.heliyon.2023.e17258
Received 8 December 2022; Received in revised form 12 June 2023; Accepted 12 June 2023
Available online 13 June 2023

from different biomass sources. Thus, we show a reliable and greener alternative chemical treatment for the obtention of MFC.

1. Introduction

Cellulose is the most abundant biomolecule in nature as it is the main component of plant cell walls. It is formed by glucose units linked by β-1,4-glycosidic bonds and structured in crystalline and amorphous regions [1]. Microfibrillated cellulose (MFC) is composed of the high crystallinity fibers of cellulose, its properties include surface area, fibrous nature, water insolubility, hydrophilicity, non-toxicity, biocompatibility, and biodegradability making it appealing for biomedicine and biotechnology applications [1]. Unlike synthetic and semisynthetic polymers that usually require the use of hazardous chemicals and elaborated processes, MFC can be obtained from lignocellulosic biomass (i.e., stems, peels, husks) using a circular bio-economy approach [2]. Hence, agricultural "waste" becomes a renewable and low-cost feedstock that can be transformed into high-value products through biological, chemical, and physical treatments [2].

Biomass-derived MFC is generally isolated using strong inorganic acids for hydrolysis. During the pretreatments, the crosslinked structure of lignocellulosic biomass is lost, increasing cellulose content on the sample, and causing an expansion of the volume (swelling). This increases the interaction between water molecules with the cellulose fraction structure, expanding the polymer surface area [3].

However, strong acid hydrolysis leads to random rupture of crystalline regions, low yields, hazardous by-product generation, and equipment corrosion [4]. Organic acids (i.e., acetic, citric, oxalic) are worth exploring as substitutes for hydrolysis due to their ease of production, safety management, low cost, and environment-friendliness [5]. Oxalic acid is the simplest dicarboxylic acid and a natural product of plant metabolism. It has been thoroughly studied in the pretreatment of lignocellulosic biomass and de-polymerization of cellulose as it affects the cellulose's amorphous regions at low concentrations, leading to high yields of crystalline structures [4]. One alternative is to integrate steam explosion pretreatment with acid hydrolysis to promote an 'auto-hydrolysis' effect on the biomass structure, leading to the proper defibrillation of cellulose fibers and their separation from lignin structures [6].

Theobroma cacao L. is an important economic species in tropical and sub-tropical countries such as Ecuador, Brazil, Ivory Coast, and Ghana, with a global cocoa bean production of over 5 million metric tons [7] to supply the ever-increasing demand in the manufacture of chocolate and cocoa products. The primary residue from cocoa industrialization is cocoa pod husk (CPH), which makes up to 72% of the fruit's total weight and comprises 35% lignin, 30% cellulose, and 10% hemicellulose [8]. However, CPH residues currently have no place in the production chain due to inappropriate waste management practices [9]; therefore, there is an opportunity for the valorization of CPH in the industry [10–13].

Few studies report cellulose isolation and characterization from CPH residues. Zailani et al. (2016) [12] reported the isolation of CPH cellulose through alkaline treatments and ultrasonication, resulting in nanocellulose with particle sizes down to 280 nm. Jimat et al. (2020) [13] detailed the isolation of cellulose nanofibers through hydrolysis with 1% sulfuric acid, producing fibers with diameters around 200–400 nm. A similar approach was followed by Akijonkun et al. (2021) [10] for the isolation of nanocellulose from CPH with sulfuric acid 64% at 45 °C, leading to polymers with a diameter of around 10–60 nm and a thermal stability temperature up to 351 °C. However, these chemo-mechanical processes produce many undesired byproducts; hence, additional downstream purification limits their economic feasibility for industrial production of MFC [14].

To date, no studies have explored greener alternatives for CPH cell wall breakdown into high-value cellulose derivatives. Furthermore, there is a need for optimized conditions to maximize extraction yields and open the feasibility for industrial applications. A design of experiments (DOE) with a response surface methodology (RSM) approach has been widely used for industrial applications to generate models for the optimization and prediction of one or several response variables when given a set of initial conditions [15]. To the best of our knowledge, there is a lack of reports that explore the implementation of such experimental design to maximize cellulose extraction yields from CPH, let alone the use of oxalic acid hydrolysis in this process. Therefore, our study aims to evaluate the use of oxalic acid for cellulose recovery from CPH through a DOE-RSM approach. Finally, this work presents a series of steps for the pretreatment of biomass that can allow the valorization and reutilization of the generated byproducts, following a green chemistry approach.

2. Materials and methods

2.1. Materials

Fresh cocoa fruits from the widely produced CCN-51 variety were kindly donated by local farmers from the San Jacinto Association in the Guayas province in Ecuador. Reagents were purchased from the following providers: Nitric acid 70% v/v (Merck, Germany), sodium hydroxide 99.9% (Merck, Germany), and sulfuric acid 96–98% v/v (Merck, Germany). Oxalic acid dihydrate 99.5% (ISO-Lab, Germany), Ethanol 96% (PanReac AppliChem, Spain), and sodium hypochlorite 10% p/v (PanReac AppliChem, Spain).

2.2. Sample preparation

Initially, CPH samples were washed by rinsing with tap water, cut into small pieces, and prepared according to the National

Renewable Energy Laboratory (NREL) procedure (LAP) 510–42620 [16]. Briefly, CPH samples were oven dried (ELOS H110F115, MEMERT, Germany) at 60 °C until constant weight, then milled and sieved (WSTYLER, United States) to #30 and #100 mesh sizes before analysis and pretreatment. Pectin was removed from CPH following Vriesmann, Teofilo, and Petkowizc (2012) [11] method. Briefly, samples with 1 mm particle size were suspended in a solution (1:25 g:mL, biomass:citric acid ratio) of 10 mM citric acid adjusted to pH 3 (APERA PH820, United States) with a solution of hydrochloric acid (HCl) 0.1 M, at 95 °C for 95 min under continuous stirring. Then, the sample was centrifuged (Hermle Z206-A, Germany) at 6000 rpm for 15 min, precipitated with EtOH 96% (1:2 v:v, biomass:ethanol ratio) for 48 h at room temperature, vacuum filtered, and dried at 60 °C until constant weight. Waxes and lipids were removed from the pectin-free CPH via Soxhlet extraction following NREL method 510–42619 [17], using water and EtOH 96% v/v as solvents for 6–8 h. The resulting extractive-free biomass (EFB) fraction (Fig. S1b) was dried and stored at room temperature until further analysis. Although not evaluated during this study, the adopted approaches allow the characterization and follow-up study of the resulting Soxhlet and pectin extracts.

2.3. Purification of the cellulose fraction

EFB samples were delignified via an alkaline treatment proposed by Lubis (2018) [18] and Obeng (2019) [19] with minor modifications. In short, EFB was treated with a 2% w/v NaOH (1:15 g:mL, biomass: liquor ratio) for 1 h in an autoclave (Hysc AC-60, Korea) at 120 °C with a sudden release of pressure. After cooling, the sample was washed with distilled water, filtered with a Buchner funnel, and bleached with 2.5% w/v NaClO (1:15 g:mL) at room temperature for 24 h. Samples were further delignified with a solution of 17.5% (w/v) NaOH (1:7 g/mL, fiber: liquor ratio) at 80 °C for 2 h and subjected to a second bleaching with a solution of 5% NaClO (1:15 g:mL) at 60 °C for 2 h. Finally, the purified cocoa cellulose (PCC) fraction (Fig. S1a) was washed with distilled water and stored at 4 °C until further analysis.

2.4. Organic acid hydrolysis optimization through a response surface methodology

PCC was subjected to acid hydrolysis proposed by Deepa et al. (2015) [20] and Mariño et al. (2018) [21] with minor modifications. The treatment consisted of a steam explosion with oxalic acid (1:15 g/mL, cellulose pulp:oxalic acid) at pre-set conditions of temperature, time, and concentration in an autoclave, with a sudden release of pressure at the end of each run. The reaction was halted by adding 10-fold cold distilled water, and then the suspension was centrifuged at 5000 rpm for 15 min. The hydrolyzed cocoa cellulose (HCC) fraction (Fig. S1c) was thoroughly washed with distilled water until reaching neutral pH, and then it was filtered on a Buchner funnel. The optimal conditions for the hydrolysis were determined by evaluating the effect of the variables described above with the yield (%) of HCC using the formula below:

$$Hydrolyzed\ cellulose\ yield\ \% = \frac{Weight_{dry\ hydrolyzed\ cellulose}}{Weight_{dry\ purified\ cellulose}}\ x\ 100 \quad (1)$$

We implemented a response surface methodology (RSM) approach to determine the optimum conditions of hydrolysis of oxalic acid concentration (5–10% w/v), reaction temperature (110°–130 °C) and reaction time (30–90 min). HCC yield was selected as the response variable (Table 1). The order of runs and independent variables' levels were generated using the Design Expert 11 Software (Stat-Ease Inc., Minneapolis, USA) (Table 2), with nineteen experimental runs carried out independently in duplicate.

Experimental points were fitted to generate a RSM prediction model, expressed as a second-order polynomial equation, evaluating the effect of each independent variable and their multiple two-way interactions on the response [15]. No transformation was applied before the statistical analysis. The quality of the model was studied by the coefficient of determination (R^2), variance coefficient, lack of fit, and analysis of variance (ANOVA).

Response surfaces were created by plotting all registered combinations between two-factor variables, whereas a third variable is fixed in a constant level, usually in the lowest or middle level. Finally, a confirmation analysis was carried out to measure the capacity of the model to generate adequate conditions on different criteria, such as achieving higher HCC yield or milder conditions of temperature, time, and acid concentration. For this study, the analysis followed time-saving criteria for HCC hydrolysis. A detailed description of the generated products and the workflow of this study can be found in the supplementary information (Fig. S2).

2.5. Characterization

2.5.1. Functional groups analysis by fourier transform infrared spectroscopy (FTIR)

Infrared spectra of samples were obtained using FTIR spectroscopy (Cary 630 FTIR spectrometer from Agilent Technologies) with a

Table 1
Experimental levels of the factor variables used in the hydrolysis process.

Symbol	Independent variable	Unit	Levels		
			−1	0	1
A	Reaction temperature	°C	110	117.5	125
B	Reaction time	min	30	60	90
C	Oxalic acid concentration	% w/v	5	7.5	10

Table 2
Design matrix and experimental results.

Run	A: Reaction Temperature (°C)	B: Reaction time (min)	C: Oxalic acid concentration (% w/v)	HCC yield (%)
1	125.0	60.0	5.0	85.4
2	125.0	60.0	10.0	68.0
3	110.0	90.0	7.7	63.7
4	110.0	90.0	10.0	52.2
5	110.0	90.0	5.0	79.9
6	117.5	60.0	7.5	83.3
7	117.5	60.0	7.5	78.8
8	117.5	30.0	5.0	86.2
9	117.5	30.0	10.0	71.4
10	110.0	36.6	5.0	81.2
11	110.0	36.6	7.7	72.1
12	110.0	36.6	10.0	62.3
13	117.5	60.0	7.5	79.6
14	117.5	60.0	7.5	81.8
15	125.0	30.0	8.1	68.2
16	125.0	30.0	5.0	78.8
17	123.4	90.0	7.4	54.3
18	123.4	90.0	5.0	68.7
19	123.4	90.0	10.0	50.3

Smart iTR module with Attenuated Total Reflectance (ATR) equipped with Microlab PC software. Spectra wave number was established between 4000 and 400 cm^{-1} at a 5 cm^{-1} resolution.

2.5.2. Thermogravimetric Analysis (TGA), derivative thermogravimetry (DTG) and Differential Scanning Calorimetry (DSC)

Thermogravimetric Analysis (TGA), Derivative Thermogravimetry (DTG), and Differential Scanning Calorimetry (DSC) determined sample thermal profile as described by Alvarez-Barreto (2021) [22]. The assay was performed in a PerkinElmer Simultaneous Thermal Analyzer STA 8000. Five milligrams of chemically treated and non-treated samples were heated from 25 °C to 600 °C, with a heating ramp of 10 °C/min and a nitrogen gas flow of 20 mL/min.

2.5.3. Crystallinity index and crystallite size analysis by X-ray diffraction (XRD)

Two methods were implemented to analyze the sample crystallinity index (CI). We used a Bruker D8 ADVANCE, ECO X-ray diffractometer, equipped with an LYNXEYE-XE detector using Cu-Kα radiation, at an angular range of 2 θ between 10 and 100°, in steps of 0.02°. The electric potential and current were kept at 25 kV and 40 mA, respectively. The traditional peak height method, based on Segal (1959) [23], uses the following equation:

$$\mathrm{CI} = \left[\frac{\mathrm{I}_{200} - \mathrm{I}_{\mathrm{am}}}{\mathrm{I}_{200}}\right] \mathrm{x}\ 100\% \tag{2}$$

where I_{200} is the total peak intensity at the position of the crystalline (200) reflection of cellulose, around 2 $\theta \approx 22.4°$, and I_{am} is the X-ray intensity of the amorphous domain, obtained at 2 $\theta \approx 18.6°$.

Based on amorphous background subtraction, the second method fits the sample amorphous contribution to the X-ray diffraction [24], which was done using the DIFFRAC. EVA software suite from Bruker. After subtracting the amorphous contribution, the crystallinity index was calculated as:

$$\mathrm{CI} = \frac{A_{peaks}}{A_{total}} \mathrm{x}\ 100\% = \frac{\int_{2\theta_1}^{2\theta_2} I_{peaks} d(2\theta)}{\int_{2\theta_1}^{2\theta_2} I_{total} d(2\theta)} \mathrm{x}\ 100\% \tag{3}$$

where $2\theta_1 = 10°$ and $2\theta_2 = 100°$, and I_{peaks} is the X-ray diffraction intensity of the crystalline peaks only, that results from subtracting the amorphous contribution from the total intensity (I_{total}) of the X-ray diffractogram. Thus, the whole area under the X-ray diffractogram is considered in this second method, not only the photons diffracted at specific angular positions.

From the X-ray diffraction data, we also estimated the cellulose crystallite size using the well-known Scherrer equation [25,26]:

$$\mathrm{L} = \frac{K\lambda}{\beta \cos\theta} \tag{4}$$

Here, L is the average size of the crystallites, $\lambda = 1.54$ Å is the radiation wavelength, β is the full width at half maximum (FWHM) of the crystalline diffraction peak (in radians) and θ its Bragg angle, *i.e.,* half the diffraction angle 2 θ (we used the main diffraction peak, thus $\theta \approx 11.2°$). Finally, K is known as the Scherrer constant, which slightly depends on the crystal shape and size distribution, although its value typically lies between 0.6 and 2. Therefore, for not very thorough estimations of the crystallite size, a value of 0.9 is generally used as a good approximation [25,26].

2.5.4. Morphology analysis by Scanning Electron Microscopy (SEM)

Surface and fiber morphologies of the samples were characterized by Scanning Electron Microscopy (SEM) using a JEOL JSM-IT300 at a voltage of 15 kV. Fibrillated regions and fractioned structures were scouted at different magnifications. We measured the average diameter of the isolated fibers and their standard deviation.

3. Results and discussion

3.1. Regression model analysis

Based on the experimental data of all three levels for A: reaction temperature (°C), B: reaction time (min), and C: oxalic acid concentration (%w/v), the following quadratic equation was generated:

$$\text{CHC yield} = 81.19 - 1.69A - 5.15B - 9.53C - 4.02AB + 1.82AC - 2BCE - 6.95A^2 - 11.69B^2 + 3.42C^2 \quad (5)$$

Positive and negative values in the equation indicate how independent variables' single or two-way interactions contribute to the response (HCC yield) [27]. The equation describes a negative influence of most variables or their interactions. This might be explained in the hydrolysis reaction because strong conditions tend to decrease the yield of the process [14].

ANOVA (Table 3) determined the significance and fitness of the generated model. All terms in the equation and prediction model contributed significantly to the HCC yield ($p < 0.05$). The p-value of the lack of fit test for the generated model was 0.6029, indicating that most of the variance has been correctly assigned to each variable or their interactions and that systematic errors are not contributing to the model, thus confirming its reliability [28]. The coefficient of variation (C.V.) and signal-noise ratio, 2.7% and 25.94, respectively, complement the lack of fit test by suggesting the model reliability for evaluating different conditions in the simulation space. Finally, the R^2 coefficient of 0.985 assesses the adequacy of the experiments acquired and how it fits the model, giving a reasonable estimate of the response variable during the process [27].

3.1.1. Interaction between hydrolysis conditions

The regression equation is described in 3D response surface plots, showing the simultaneous dependence of HCC yield on the reaction conditions (Fig. 1). The model indicates that high yields (>70%) can be reached when evaluating low levels of oxalic acid concentration (Fig. 1a). The acid used for the hydrolysis process has the most critical role, as it defines the final structure of the composite, its dimension, surface area, and functionalization [29]. As for the reaction temperature and time (Fig. 1b), the model revealed high yields at middle levels (116–119 °C, 50–60 min). High temperatures during hydrolysis allow the catalyst to reach more accessible and disordered regions while leaving crystalline regions free [30], as it surpasses the thermic energy needed to break the strong bonds between cellulose chains [28]. Simultaneously, time plays a vital role (Fig. 1c) in leading the correct chemical degradation of cellulose chains by allowing the diffusion and penetration of the catalyst into the cellulosic matrix [27]. It is worth noting that an increase in the hydrolysis time, temperature, and acid concentration leads to an abrupt yield reduction. This is more evident in the oxalic acid concentration, where high concentrations lead to the lowest yields (<50%). This is due to the chemical degradation of the cellulose structure, which is transformed into simpler molecules like glucose and other polysaccharides.

During the confirmation analysis, following time-saving criteria, the optimization model selected the hydrolysis conditions of 125 °C, 30 min, and an oxalic acid concentration of 5% w/v. The predicted HCC yield for these conditions was 79.17%, whereas the

Table 3
ANOVA analysis of the generated quadratic model based on a 95% confidence interval. Significant factors were selected based on F-value (>1) and p-value (<0.005). The lack of fit term expresses the relation between residual and pure error values, where an insignificant value indicates the low influence of external factors over the generated model. Variance coefficient (C.V.) estimates the relation between the variability and the data mean, indicating the precision of a model.

Source	Sum of Squares	df	Mean Square	F-value	p-value	
Model	2248.58	9	249.84	65.42	<0.0001	significant
A-Reaction temperature	32.03	1	32.03	8.39	0.0177	
B-Reaction time	297.82	1	297.82	77.98	<0.0001	
C-Oxalic acid concentration	975.70	1	975.70	255.47	<0.0001	
AB	128.41	1	128.41	33.62	0.0003	
AC	26.42	1	26.42	6.92	0.0274	
BC	31.99	1	31.99	8.38	0.0178	
A^2	142.16	1	142.16	37.22	0.0002	
B^2	401.55	1	401.55	105.14	<0.0001	
C^2	41.92	1	41.92	10.97	0.0090	
Residual	34.37	9	3.82			
Lack of Fit	21.71	6	3.62	0.8568	0.6029	not significant
Pure Error	12.67	3	4.22	R^2	0.9849	
Std. Dev.	1.95			Adjusted R^2	0.9699	
Mean	71.91			Predicted R^2	0.9375	
C.V. %	2.72			Adequate Precision	25.9369	

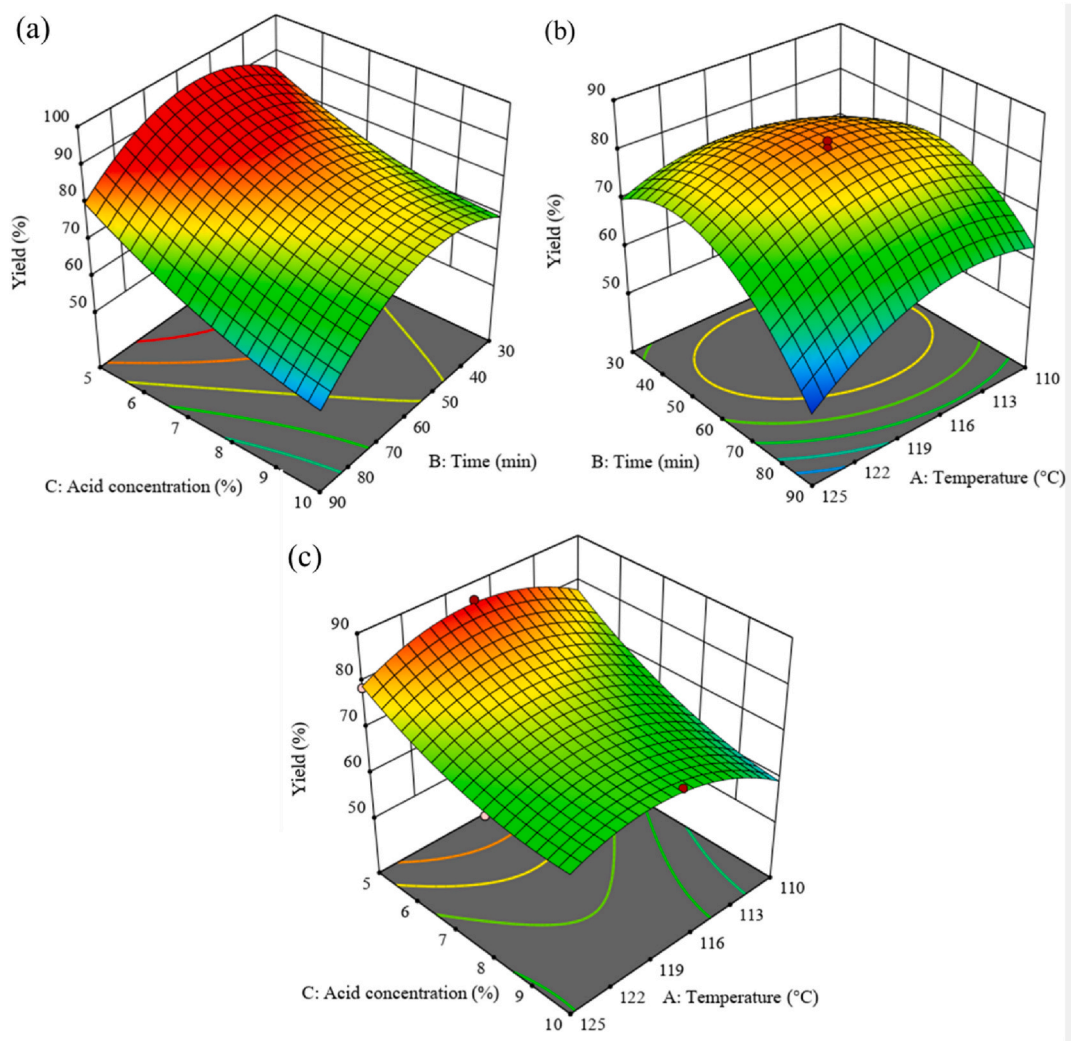

Fig. 1. Response surface for the interaction between entry factors, based on the 3D plotting of all combinations of two variables while keeping a third one in a constant value for evaluation. (a) Reaction temperature vs reaction time, at a constant oxalic acid concentration of 7.5% w/v. (b) Oxalic acid concentration and reaction time at a constant temperature of 116.45 °C. (c) oxalic acid concentration and reaction temperature at 30 min.

experimental yield was 75.7% (Table S1). The obtained optimal yield was higher than previous studies focused on cellulose polymers isolation from African Napier grass (52%) [31], Kans grass (72.3%) [14], and similar to the one obtained from tea waste (86.7%) [30].

3.2. *Functional groups analysis by fourier transform infrared spectroscopy (FT-IR)*

FTIR spectra (Fig. 2) revealed similar results compared to previous studies on the characterization of the CPH [10,32]. However, some differences were found in the intensity of the signals (Table S2) associated with the conditions of the performed chemical treatments and the geographic origin of the sample. All three sample spectra showed a broad band at 3326 cm^{-1} and peaks in regions around 1638-1608 cm^{-1}, attributed to the O–H stretch of hydroxyl groups and O–H bonds from absorbed moisture [33]. Non-cellulosic components were detected in the FTIR spectra of EFB, such as a peak at 1727 cm^{-1}, associated with the stretch of C=O bonds from hemicellulose carboxyl groups [32], and a signal at 1244 cm^{-1} attributed to C–O groups from acetyl groups in lignin [10]. These signals were lower in PCC samples, whereas HCC spectra didn't detect these groups, indicating that the chemical treatment allowed the removal of hemicellulose and lignin from the sample.

All three samples generated signals at 2895 and 1028 cm^{-1}, attributed to the stretch of C–H bonds in cellulose chains [32]. The peaks at 1430, 1370, and 1318 cm^{-1} indicate the presence of C–H bonds of carbohydrates [10] with increasing intensities after each chemical treatment due to the high cellulose content in PCC and HCC samples. Finally, the spectra revealed peaks at 1110 and 901 cm^{-1}, depicted as the C–O–C stretching of pyranose rings and the stretch of C–H bonds from glucose rings in the cellulose chain,

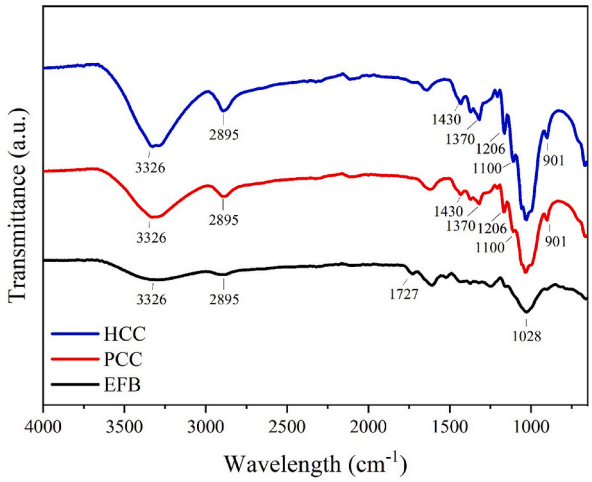

Fig. 2. FTIR spectra for the EFB, PCC and HCC samples. The intensity of the signals in different wavelength reveals the presence of relevant molecular groups found in the main structural polymers of the sample.

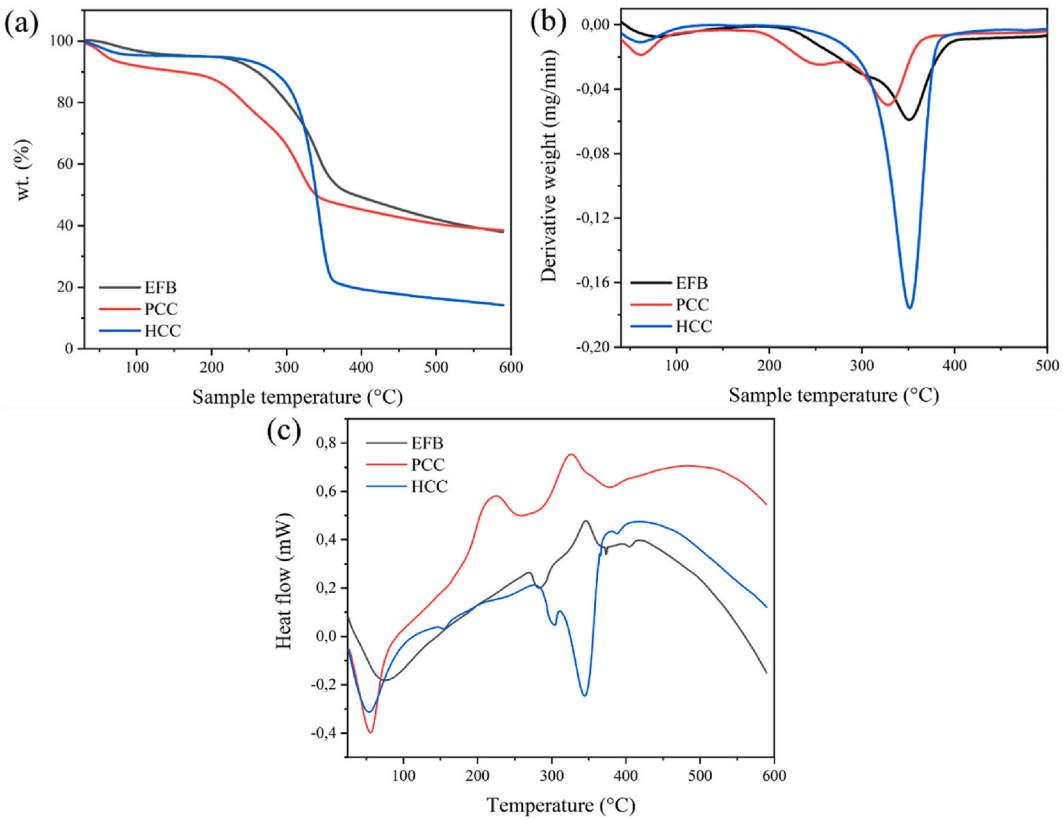

Fig. 3. Thermal profile for EFB, PCC, and HCC samples. (a) Thermogravimetric analysis (TGA) curves indicate the thermic degradation regions of the main compounds present in biomass samples. (b) Differential thermogravimetric (DTG) curves, reveals the thermal degradation rate of treated samples (c) Differential Scanning Calorimetry (DSC) curves specify the heat flow of the biomass sample on response to temperature increase, allowing the identification of degradation temperatures, transition temperature and the presence of possible residues.

confirming the presence of purified cellulose structures in the sample [32,33].

3.3. Thermogravimetric Analysis (TGA), derivative thermogravimetry (DTG) and Differential Scanning Calorimetry (DSC)

The TGA and Derivative thermogravimetry (DTG) curves revealed three regions of degradation (Fig. 3a and b). The first region of thermal decomposition was registered at 78.7 °C for EFB, and 61.3 °C for PCC and HCC. It is linked to the vaporization of moisture and volatilization of low molecular weight compounds [10,33]. The second region was revealed between 255 and 300 °C in all three samples and is related to hemicellulose degradation. PCC samples registered a strong signal at 255 °C, showing the presence of hemicellulose residues after the alkaline and bleaching treatments. In EFB, this signal overlapped due to the joint degradation of hemicellulose and low molecular weight components associated with the lignin [34]. Finally, HCC's signal at this region was absent as hemicellulose was removed during hydrolysis.

The last main region of thermal degradation was recorded between 328 and 350 °C, depicting cellulose degradation from the sample [34]. DTG curves of EFB and HCC revealed a degradation peak at 350 and 351 °C, respectively, with a stronger signal in the hydrolyzed sample due to its higher cellulose content. PCC recorded a maximum thermal stability temperature of 328 °C, related to non-cellulosic residues in the sample [10]. The DTG curve of HCC revealed a maximum stability temperature of 351 °C, indicating its high thermal stability. HCC maximum degradation temperature is higher than those reported for MFC isolated from kans grass (340 °C) [14], napier grass (300 °C) [31], roselle fibers (326 °C) [35], and tea waste (300 °C) [30], lower than those reported from olive (380 °C) [35] and conocarpus (408 °C) [36] fibers and similar to what Akinjokun (2021) [10] reported on nanocellulose isolated from CPH (350 °C).

DSC diagrams of EFB, PCC, and HCC samples showed regions of thermal degradation (Fig. 3c). The first endotherm was detected at

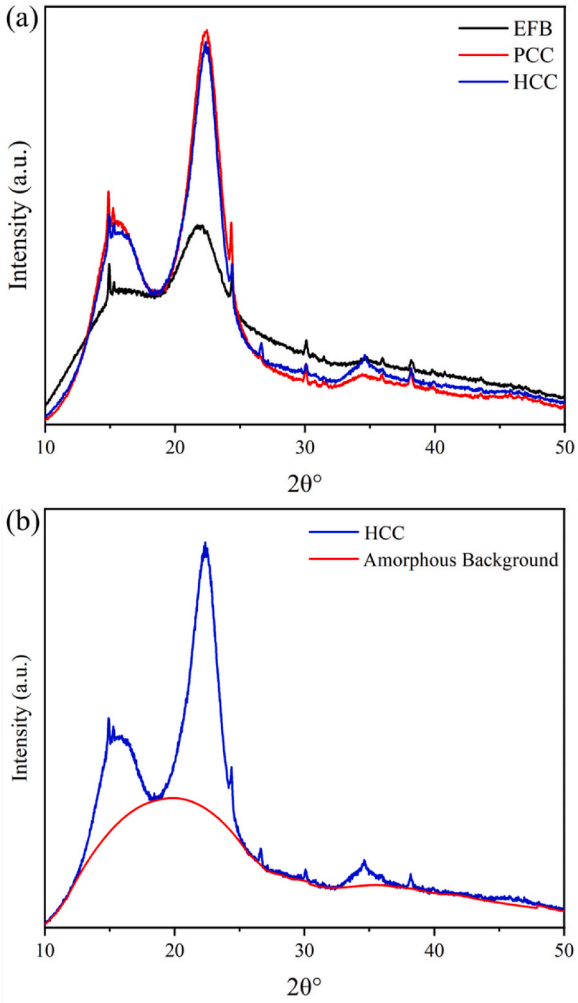

Fig. 4. (a) X-ray diffractograms for the EFB, PCC, and HCC samples. (b) Sample crystallinity index measured through the amorphous subtraction method, where the generated model fits the amorphous contribution to the overall signal.

56 °C for PCC and HCC samples and 77 °C for EFB, related to water loss and volatile compounds degradation [10,33,37]. EFB samples registered an exothermic peak at 227 °C and an endothermic peak at 283 °C, related to the degradation of hemicellulose and the thermic de-polymerization of the sample, respectively [38]. PCC samples revealed a similar peak around 227–255 °C, suggesting the presence of residual hemicellulose. Finally, the analysis revealed at 327 and 346 °C, for EFB and PCC, respectively, related cellulose and lignin degradation [36]. HCC samples showed a slight endotherm at 154 °C, associated with the glass transition temperature of cellulose and a change in its structure due to the temperature [39]. Two endothermic peaks were registered at 303 °C and 345 °C. These

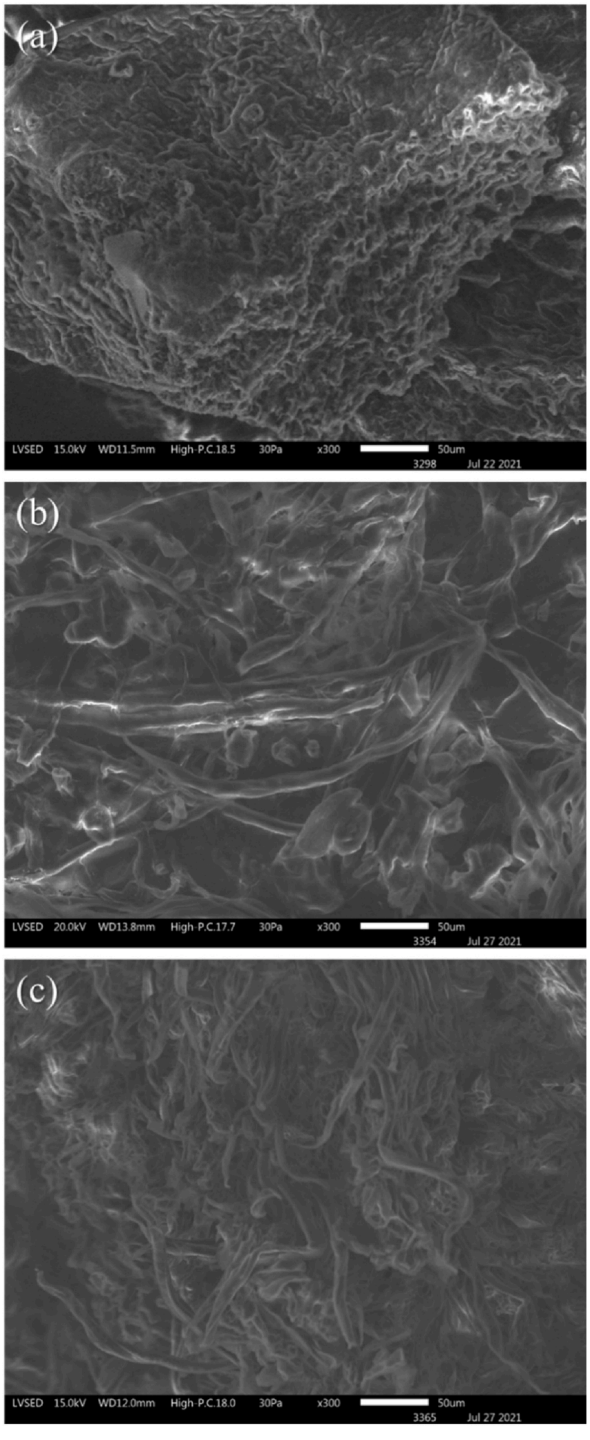

Fig. 5. SEM images of (a) EFB, (b) PCC, and (c) HCC.

peaks represent the melting and depolymerization of cellulose structures with high crystallinity. Similar endotherms and temperatures were discussed to isolate MFC and nanocellulose from a lignocellulosic biomass [36,40]. The peak registered at 303 °C could be associated with a hornification effect, where cellulose irreversibly agglomerates, reducing its degree of polymerization and thermal stability [41]. HCC thermal properties allow its use in manufacturing processes, which exhibit rapid temperature changes, increasing the need for thermally stable materials [42].

3.4. Crystallinity index and crystallite size analysis by X-ray diffraction (XRD)

X-ray diffractograms of chemically-treated samples (Fig. 4a) revealed three prominent diffraction peaks at $2\Theta \approx 15.6°$, 22.4°, and 34.6°, related to the crystallographic planes (110), (200), and (004) of cellulose I polymorph [10]. Cellulose I consists of analogous polysaccharide chains composed of Ia and Ib allomorphs, whose physical properties depend on the concentration of these allomorphs [1]. EFB high content of non-cellulosic components resulted in a low CI of 33.1% (peak height method) and 12.3% (amorphous subtraction method). But as chemical treatments progress, the intensity of the diffraction peaks increase and become narrower [10,20]. CI for both PCC and HCC increased up to 64.7% and 63.4% (peak height method) and 33.4% and 29.0% (amorphous subtraction method), respectively, due to the rupture of the crosslinking between cellulose, lignin, and hemicellulose [43]. The similarity between these two samples might be related to the hydrolysis conditions, incapable of hydrolyzing the amorphous content of the cellulose structures and thus not increasing the crystallinity of the sample. On the other hand, the hydrolysis demonstrated an improvement of HCC thermal properties and a low content of non-cellulosic components based on the TGA, DSC, and FTIR analysis.

As it is well known, the Segal's peak height method revealed a significant overestimation of the CI for all the samples compared to the amorphous subtraction method [24]. This is because the mass fractions of amorphous and crystalline material are related to the area under the X-ray diffractograms and not the intensity in a single diffraction angle. On the other hand, the difficulty of the amorphous subtraction method resides in determining the contribution from the amorphous regions to the XRD intensity (see example in Fig. 4b) [24].

Notwithstanding the difficulties inherent to the methods for the structural analysis of organic materials such as cellulose, it is essential to consider their complementary contribution to microcellulose isolation studies. When comparing our results with other studies, based on the peak height method, the CI of PCC and HCC stood in close range with sulfuric acid hydrolyzed CPH nanocellulose (67.6%) [10].

Upon evaluating the crystallite sizes with the Scherrer equation based on the XRD diffractogram peaks, the samples revealed morphologies of 2.8, 3.4, and 3.7 nm for the EFB, PCC, and HCC samples, respectively. It is worth noting that the Scherrer equation works with the inverse proportionality between the peak width and the approximate crystallite size. However, it considers all crystallites as stress-free, uniform, and dimensional similar structures [44]; thus, its usefulness resides in comparing treated and untreated samples. The crystallite sizes correlate very well with the CI results. The PCC and HCC samples present very similar results due to the hydrolysis conditions' inability to change the crystal properties of the isolated cellulose polymer and with crystallite sizes larger than that for the poorly crystallized EFB sample. Also, the calculated crystallite sizes are smaller than those estimated on cellulose isolated from cactus (6 nm) [44], but comparable to the values obtained for dunchi fiber (4 nm) [45].

3.5. Morphology analysis by scanning electron microscopy (SEM)

The EFB micrograph showed a porous surface morphology with no individual fiber structures found (Fig. 5a) due to the crosslinking and cementation of cellulose fibers caused by hemicellulose and lignin [10]. Alkaline and bleaching pretreatments allowed the delignification and defibrillation of cellulose structures into individual fibers [31,46]. The PCC (Fig. 5b) micrograph reveals several individual fiber structures, with an average diameter of 13.2 ± 1.8 μm (Fig. S3a) and agglomerate areas linked to cellulose separate structures [10,47] and hemicellulose residues, similar to what the TGA revealed.

HCC micrograph (Fig. 5c) revealed several individual fibers and less agglomerated areas than PCC, related to the acid hydrolysis process, which removes the amorphous regions of cellulose chains and reduces their particle size. In this case, the average diameter of the individual fibers was decreased to 8.5 ± 1.7 μm (Fig. S3b). The resulting dimensions proved to be lower than the fibers isolated from Roselle fiber [35] and corncob [48] with fiber diameters of 44.28 and 83 μm respectively. It is worth noting that the rough surfaces and heavy agglomerate areas found in PCC and HCC samples might be related to the hornification effect, which revealed anomalous peaks on the DSC curves.

4. Conclusion

In this study, a green chemistry protocol using oxalic acid hydrolysis is designed and optimized to isolate MFC fibers from CPH. Optimum conditions for time-saving criteria were 125 °C, 30 min at 5% w/v acid concentration, with an experimental yield of 75.7%. Characterization analysis revealed a microcellulose polymer with a thermal stability of up to 350 °C, 29.0 %CI, and fibrous morphologies of 8.5 μm average diameter. The isolated MFC properties are similar to other biomass-based cellulose polymers obtained through inorganic acid hydrolysis, therefore, serving as a replacement for the lignocellulosic residual biomass hydrolysis. Cocoa biomass valorization might promote the generation of a bioeconomy, diversifying sensible agroindustries, creating new jobs, and improving the overall living conditions of the rural communities that depend on farm activities.

Author contribution statement

Luis-Fernando Zambrano: Conceived and designed the experiments; Performed the experiments; Analyzed and interpreted the data; Wrote the paper.

Yanet Villasana: Conceived and designed the experiments; Analyzed and interpreted the data; Contributed reagents, materials, analysis tools or data.

M. Lorena Bejarano, Christian Luciani, Darío Niebieskikwiat, Willin Álvarez: Analyzed and interpreted the data.

Dario F. Cueva: Analyzed and interpreted the data; Contributed reagents, materials, analysis tools or data.

Daniel Aguilera-Pesantes: Contributed reagents, materials, analysis tools or data.

Lourdes M. Orejuela-Escobar: Conceived and designed the experiments; Contributed reagents, materials, analysis tools or data.

Data availability statement

Data will be made available on request.

Declaration of competing interest

The authors declare that they have no known competing financial interests or personal relationships that could have appeared to influence the work reported in this paper.

Acknowledgments

The authors would like to thank the personnel from the USFQ's Department of Chemical Engineering, particularly the Applied Circular Engineering and Simulation Research Group (GICAS) and Jose Alvarez-Barreto. We are also thankful to personnel at the Mechanical Engineering Department, and the Institute of Materials Research Laboratory of the Universidad San Francisco de Quito. We would also like to thank Doménica Vargas, Patricia Torres, Kherlyn Bajaña, and Carlos Bajaña for their logistical support. We thank the local cocoa farmers, who kindly provided CPH for our assays. Clydent Co. Ltd., and Universidad San Francisco de Quito sponsored this work.

Appendix A. Supplementary data

Supplementary data to this article can be found online at https://doi.org/10.1016/j.heliyon.2023.e17258.

References

[1] Z.N. Garba, I. Lawan, W. Zhou, M. Zhang, L. Wang, Z. Yuan, Microcrystalline cellulose (MCC) based materials as emerging adsorbents for the removal of dyes and heavy metals – a review, Sci. Total Environ. 717 (2020), 135070, https://doi.org/10.1016/j.scitotenv.2019.135070.

[2] L.M. Orejuela-Escobar, A.C. Landázuri, B. Goodell, Second generation biorefining in Ecuador: circular bioeconomy, zero waste technology, environment and sustainable development: the nexus, J. Bioresour. Bioprod. 6 (2021) 83–107.

[3] F. Camacho, P. González-Tello, E. Jurado, A. Robles, Microcrystalline-cellulose hydrolysis with concentrated sulphuric acid, J. Chem. Technol. Biotechnol. Int. Res. Process. Environ. Clean Technol. 67 (1996) 350–356, https://doi.org/10.1002/(SICI)1097-4660 (199612)67:4<350::AID-JCTB564>3.0.CO;2-9.

[4] W. Xu, H. Grénman, J. Liu, D. Kronlund, B. Li, P. Backman, J. Peltonen, S. Willför, A. Sundberg, C. Xu, Mild oxalic-acid-catalyzed hydrolysis as a novel approach to prepare cellulose nanocrystals, ChemNanoMat 3 (2017) 109–119, https://doi.org/10.1002/cnma.201600347.

[5] M.A. Mariño, D. Cypriano, L. Tasic, Agroindustry residues as a source for cellulose nanofibers production, J. Braz. Chem. Soc. 32 (2021) 878–888, https://doi.org/10.21577/0103-5053.20200239.

[6] M.A. Dahlem, C. Borsoi, B. Hansen, A.L. Catto, Evaluation of different methods for extraction of nanocellulose from yerba mate residues, Carbohydr. Polym. 218 (2019) 78–86, https://doi.org/10.1016/j.carbpol.2019.04.064.

[7] D. Ghosh, The top cocoa producing countries in the world, World (2022). https://www.worldatlas.com/industries/the-top-cocoa-producing-countries-in-the-world.html.

[8] F. Lu, J. Rodriguez-Garcia, I. Van Damme, N.J. Westwood, L. Shaw, J.S. Robinson, G. Warren, A. Chatzifragkou, S.M. Mason, L. Gomez, Valorisation strategies for cocoa pod husk and its fractions, Curr. Opin. Green Sustain. Chem. 14 (2018) 80–88.

[9] N. Julián, C. Pardo, A. Darghan, M. Darío, S. Rico, A. Rodriguez, Spatial analysis of diseases incidence in different cocoa genotypes (theobroma cacao L.) in yopal (casanare), Colombia, Acta Biol. Colomb. (2016), https://doi.org/10.15446/abc.v22n2.61161.

[10] A.I. Akinjokun, L.F. Petrik, A.O. Ogunfowokan, J. Ajao, T.V. Ojumu, Isolation and characterization of nanocrystalline cellulose from cocoa pod husk (CPH) biomass wastes, Heliyon 7 (2021), e06680, https://doi.org/10.1016/j.heliyon.2021.e06680.

[11] L.C. Vriesmann, R.F. Teófilo, C. Lúcia de Oliveira Petkowicz, Extraction and characterization of pectin from cacao pod husks (Theobroma cacao L.) with citric acid, LWT–Food Sci. Technol. (2012), https://doi.org/10.1016/j.lwt.2012.04.018.

[12] I.S.A. Zailani, Aviceena, D.N. Jimat, M.S. Jami, Extraction of microcrystalline cellulose (MCC) from cocoa pod husk via alkaline pretreatment combined with ultrasonication, Int. J. Appl. Eng. Res. 11 (2016) 9876–9879.

[13] D.N. Jimat, S.S.S. Putra, P. Jamal, W.M.F.W. Nawawi, Isolation of nanocellulose fibers (NCF) from cocoa pod (theobroma cacao L.) via chemical treatment combined with ultrasonication, Adv. Nanotechnol. Its Appl. (2020) 97–105. https://link.springer.com/chapter/10.1007/978-981-15-4742-3_6.

[14] J. Baruah, R.C. Deka, E. Kalita, Greener production of microcrystalline cellulose (MCC) from Saccharum spontaneum (Kans grass): statistical optimization, Int. J. Biol. Macromol. 154 (2020) 672–682, https://doi.org/10.1016/j.ijbiomac.2020.03.158.

[15] D.C. Montgomery, Design and Analysis of Experiments, tenth ed., 2019.

[16] B. Hames, R.O. Ruiz, C. Scarlata, A. Sluiter, J. Sluiter, D. Templeton, D. of Energy, Preparation of Samples for Compositional Analysis, 2004.

[17] A.A. Sluiter, R. Ruiz, C. Scarlata, J. Sluiter, D. Templeton, Determination of Extractives in Biomass: Laboratory Analytical Procedure (LAP); Issue Date 7/17/2005 - 42619.Pdf, 2008. Tech. Rep. NREL/TP-510-42619.
[18] M. Lubis, A. Gana, S. Maysarah, M.H.S. Ginting, M.B. Harahap, Production of bioplastic from jackfruit seed starch (Artocarpus heterophyllus) reinforced with microcrystalline cellulose from cocoa pod husk (Theobroma cacao L.) using glycerol as plasticizer, IOP Conf. Ser. Mater. Sci. Eng. 309 (2018), https://doi.org/10.1088/1757-899X/309/1/012100.
[19] A.K. Obeng, D. Premjet, S. Premjet, Combining autoclaving with mild alkaline solution as a pretreatment technique to enhance glucose recovery from the invasive weed chloris barbata, Biomolecules (2019), https://doi.org/10.3390/biom9040120.
[20] B. Deepa, E. Abraham, N. Cordeiro, M. Mozetic, A.P. Mathew, K. Oksman, M. Faria, S. Thomas, L.A. Pothan, Utilization of various lignocellulosic biomass for the production of nanocellulose: a comparative study, Cellulose (2015), https://doi.org/10.1007/s10570-015-0554-x.
[21] M.A. Mariño, C.A. Rezende, L. Tasic, A multistep mild process for preparation of nanocellulose from orange bagasse, Cellulose 25 (2018) 5739–5750, https://doi.org/10.1007/s10570-018-1977-y.
[22] J.F. Alvarez-Barreto, F. Larrea, M.C. Pinos, J. Benalcázar, D. Oña, C. Andino, D.A. Viteri, M. Leon, D. Almeida-Streitwieser, Chemical pretreatments on residual cocoa pod shell biomass for bioethanol production, Rev. Bionatura. (2021), https://doi.org/10.21931/RB/2020.06.01.9.
[23] L. Segal, J.J. Creely, A.E. Martin, C.M. Conrad, An empirical method for estimating the degree of crystallinity of native cellulose using the X-ray diffractometer, Textil. Res. J. (1959), https://doi.org/10.1177/004051755902901003.
[24] P. Ahvenainen, I. Kontro, K. Svedström, Comparison of sample crystallinity determination methods by X-ray diffraction for challenging cellulose I materials, Cellulose (2016), https://doi.org/10.1007/s10570-016-0881-6.
[25] U. Holzwarth, N. Gibson, The Scherrer equation versus the Debye-Scherrer equation, Nat. Nanotechnol. (2011), https://doi.org/10.1038/nnano.2011.145.
[26] P. Scherrer, Göttinger nachrichten math, Phys. 2 (1918) 98–100.
[27] M. Yahya, Y.W. Chen, H.V. Lee, C.C. Hock, W.H.W. Hassan, A new protocol for efficient and high yield preparation of nanocellulose from elaeis guineensis biomass: a response surface methodology (RSM) study, J. Polym. Environ. 27 (2019) 678–702, https://doi.org/10.1007/s10924-019-01373-7.
[28] Y.W. Chen, H.V. Lee, S. Bee, A. Hamid, Investigation of optimal conditions for production of highly crystalline nanocellulose with increased yield via novel Cr (III) -catalyzed hydrolysis : response surface methodology, Carbohydr. Polym. 178 (2017) 57–68, https://doi.org/10.1016/j.carbpol.2017.09.029.
[29] J.R.A. Pires, V.G.L. Souza, A.L. Fernando, Valorization of energy crops as a source for nanocellulose production – current knowledge and future prospects, Ind. Crop. Prod. (2019), https://doi.org/10.1016/j.indcrop.2019.111642.
[30] T. Zhao, Z. Chen, X. Lin, Z. Ren, B. Li, Y. Zhang, Preparation and characterization of microcrystalline cellulose (MCC) from tea waste, Carbohydr. Polym. 184 (2018) 164–170, https://doi.org/10.1016/j.carbpol.2017.12.024.
[31] K.O. Reddy, C.U. Maheswari, M.S. Dhlamini, B.M. Mothudi, V.P. Kommula, J. Zhang, J. Zhang, A.V. Rajulu, Extraction and characterization of cellulose single fibers from native african napier grass, Carbohydr. Polym. 188 (2018) 85–91, https://doi.org/10.1016/j.carbpol.2018.01.110.
[32] M. Adjin-Tetteh, N. Asiedu, D. Dodoo-Arhin, A. Karam, P.N. Amaniampong, Thermochemical conversion and characterization of cocoa pod husks a potential agricultural waste from Ghana, Ind. Crop. Prod. 119 (2018) 304–312, https://doi.org/10.1016/j.indcrop.2018.02.060.
[33] K.S. Chun, S. Husseinsyah, H. Osman, Development of biocomposites from Cocoa pod husk and Polypropylene: effect of filler content and 3-aminopropyltriethoxylsilane, Polym. Renew. Resour. 5 (2014) 139–156, https://doi.org/10.1177/204124791400500401.
[34] R.K. Basak, S.G. Saha, A.K. Sarkar, M. Saha, N.N. Das, A.K. Mukherjee, Thermal properties of jute constituents and flame retardant jute fabrics, Textil. Res. J. (1993), https://doi.org/10.1177/004051759306301107.
[35] L.K. Kian, M. Jawaid, H. Ariffin, O.Y. Alothman, Isolation and characterization of microcrystalline cellulose from roselle fibers, Int. J. Biol. Macromol. 103 (2017) 931–940, https://doi.org/10.1016/j.ijbiomac.2017.05.135.
[36] H. Fouad, L.K. Kian, M. Jawaid, M.D. Alotaibi, O.Y. Alothman, M. Hashem, Characterization of microcrystalline cellulose isolated from conocarpus fiber, Polymers 12 (2020) 1–11, https://doi.org/10.3390/polym12122926.
[37] L.K. Kian, N. Saba, M. Jawaid, H. Fouad, Characterization of microcrystalline cellulose extracted from olive fiber, Int. J. Biol. Macromol. 156 (2020) 347–353, https://doi.org/10.1016/j.ijbiomac.2020.04.015.
[38] M.I.G. Miranda, C.I.D. Bica, S.M.B. Nachtigall, N. Rehman, S.M.L. Rosa, Kinetical thermal degradation study of maize straw and soybean hull celluloses by simultaneous DSC-TGA and MDSC techniques, Thermochim. Acta 565 (2013) 65–71, https://doi.org/10.1016/j.tca.2013.04.012.
[39] P.K. Sappati, B. Nayak, G.P. van Walsum, Effect of glass transition on the shrinkage of sugar kelp (Saccharina latissima) during hot air convective drying, J. Food Eng. (2017), https://doi.org/10.1016/j.jfoodeng.2017.04.018.
[40] A. Mandal, D. Chakrabarty, Isolation of nanocellulose from waste sugarcane bagasse (SCB) and its characterization, Carbohydr. Polym. 86 (2011) 1291–1299, https://doi.org/10.1016/j.carbpol.2011.06.030.
[41] L. Salmén, J.S. Stevanic, Effect of drying conditions on cellulose microfibril aggregation and hornification, Cellulose 25 (2018) 6333–6344, https://doi.org/10.1007/s10570-018-2039-1.
[42] D. Haldar, M.K. Purkait, Micro and nanocrystalline cellulose derivatives of lignocellulosic biomass: a review on synthesis, applications and advancements, Carbohydr. Polym. (2020), https://doi.org/10.1016/j.carbpol.2020.116937.
[43] D.C. Meza-Sepúlveda, A.M. Castro, A. Zamora, J.W. Arboleda, A.M. Gallego, A.V. Camargo-Rodríguez, Bio-based value chains potential in the management of cacao pod waste in Colombia, a case study, Agronomy (2021), https://doi.org/10.3390/agronomy11040693.
[44] C. Orrabalis, D. Rodríguez, L.G. Pampillo, C. Londoño-Calderón, M. Trinidad, R. Martínez-García, Characterization of nanocellulose obtained from cereus forbesii (a South american cactus), Mater. Res. (2019), https://doi.org/10.1590/1980-5373-MR-2019-0243.
[45] M.N. Khan, N. Rehman, A. Sharif, E. Ahmed, Z.H. Farooqi, M.I. Din, Environmentally benign extraction of cellulose from dunchi fiber for nanocellulose fabrication, Int. J. Biol. Macromol. (2020), https://doi.org/10.1016/j.ijbiomac.2020.02.333.
[46] X.Q. Chen, X.Y. Deng, W.H. Shen, M.Y. Jia, Preparation and characterization of the spherical nanosized cellulose by the enzymatic hydrolysis of pulp fibers, Carbohydr. Polym. 181 (2018) 879–884, https://doi.org/10.1016/j.carbpol.2017.11.064.
[47] J. Pennells, I.D. Godwin, N. Amiralian, D.J. Martin, Trends in the production of cellulose nanofibers from non-wood sources, Cellulose 27 (2020) 575–593, https://doi.org/10.1007/s10570-019-02828-9.
[48] X. Shao, J. Wang, Z. Liu, N. Hu, M. Liu, Y. Xu, Preparation and characterization of porous microcrystalline cellulose from corncob, Ind. Crop. Prod. 151 (2020) 1–6, https://doi.org/10.1016/j.indcrop.2020.112457.